# Surface Deformation at the Salton Sea Geothermal Field From High-Precision Radar Interferometry

**Mariana Eneva[1], David Adams[1], Giacomo Falorni[2], Fabrizio Novali[3], and Vicky Hsiao[2]**

[1]Imageair Inc., Reno, Nevada, USA
[2]TRE Canada Inc., Vancouver, BC, Canada
[3]TRE. s.r.l., Milan, Italy,
meneva@imageair-inc.com • giacomo.falorni@trecanada.com • tre@treuropa.com

***Keywords***

*Geothermal, Salton Sea, Imperial Valley, surface deformation, subsidence, InSAR, SqueeSAR, PSInSAR, radar interferometry, CalEnergy, Hudson Ranch, EnergySource*

## ABSTRACT

Interferometric synthetic aperture radar (InSAR) is applied to data from the TerraSAR-X (TSX) satellite, collected in the period August 2012 – October 2013 in the area of the Salton Sea geothermal field in southern California, for the purpose of detecting surface deformation. These data are from a new generation of satellites, with much improved spatial resolution and frequency of temporal coverage than earlier satellites like Envisat (2003-2010). The particular technique applied, SqueeSAR$^{TM}$, uses permanent and distributed scatterers, which makes it possible to observe deformation in agricultural areas, where conventional InSAR does not work. Surface deformation is first obtained in the line-of-sight (LOS) to the satellite from two orbital geometries, descending and ascending. The two LOS measurements are then used to calculate horizontal and vertical displacements. The TSX deformation time series and annual rates are compared with those previously derived from Envisat. The periods covered by the two satellites present an unprecedented opportunity to observe ongoing post-production surface deformation at the CalEnergy units of the geothermal field, operated since early 1980's, and both pre- and post-production deformation at the new Hudson Ranch-1 (HR-1) development of EnergySource, which started in early 2012. Two subsidence bowls at the CalEnergy units have been confirmed by the TSX results, similar to earlier Envisat observations, with annual subsidence rates of up to –30 mm/year relative to a benchmark on Obsidian Butte (S-1246). However, there is a clear difference between the pre- and post-production periods at the new HR-1 development, with a relative uplift (compared to S-1246) turning into a subsidence of up to –18 mm/year. Nonetheless, the possibility for anthropogenic origin of the surface deformation at this field is challenged by non-anthropogenic factors associated with the regional and local tectonics, as well as the receding Salton Sea.

## 1. Study Area

The Salton Sea geothermal field is one of four operating geothermal fields in Imperial Valley of southern California (Figure 1).

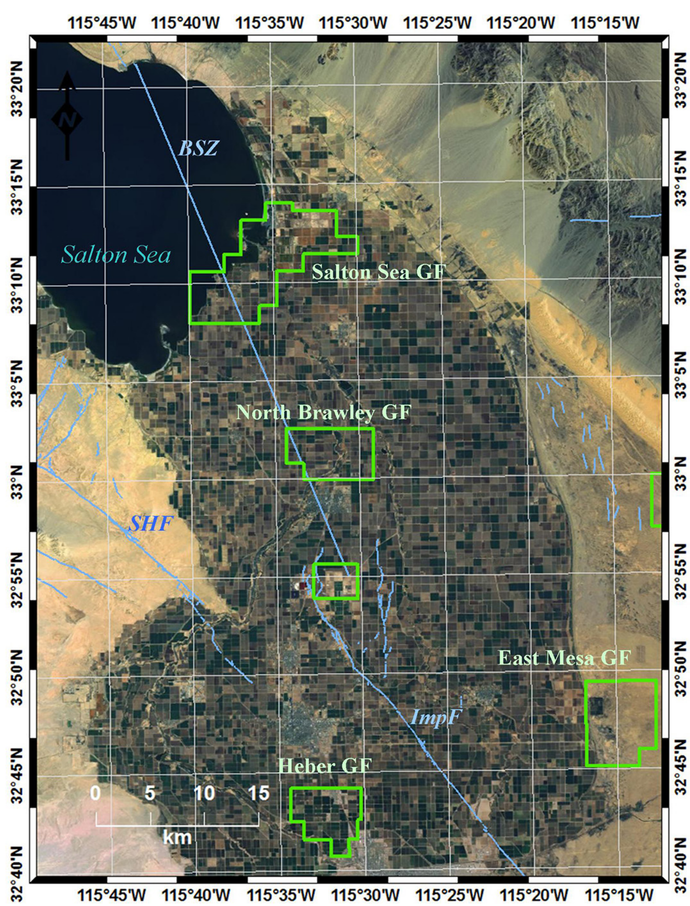


**Figure 1.** Geothermal areas in Imperial Valley in Southern California (green polygons). Names show operating geothermal fields (GF). The field south of North Brawley is not active (formerly Mesquite, or South Brawley). Blue traces denote faults and assumed fault zones (USGS). *BSZ* - center of the wide Brawley Seismic Zone, *SHF* - Superstition Hills Fault, *ImpF* - Imperial Fault. Superimposed on a satellite image.

The southwestern and central areas of the field have been operated by CalEnergy since the early 1980's (327 MW of generating capacity from 10 plants). In early 2012 EnergySource LLC started operating the Hudson Ranch – 1 (HR-1) development (49.9 MW) to the northeast of the CalEnergy units. Both developments still occupy only a small portion of the Salton Sea KGRA, which extends under large part of the Salton Sea and surrounding areas. Its mean capacity is 2210 MW, as estimated by USGS (Williams et al., 2008).

The Imperial Valley is part of the Salton Trough, which is a spreading center due to the relative movement of the Pacific and North American Plates. It is characterized by active regional tectonics, causing widespread subsidence and horizontal movements, as well as by a high heat flow giving rise to the geothermal fields. Local sources of deformation are represented by networks of strike-slip and normal faults (e.g., Brothers et al., 2009; Crowell et al., 2013), many of which are either buried or covered by agriculture. The Salton Trough also experiences abrupt surface deformation due to moderate to large earthquakes, as well as triggered or independently occurring aseismic slip (e.g., Rymer et al., 2002; Wei et al., 2009, 2011).

## 2. Technique

The method used for mapping surface deformation in Imperial Valley is satellite radar interferometry, also known as interferometric synthetic aperture radar (InSAR). SAR data suitable for interferometry have been available from several satellites so far – the European ERS and Envisat, the Canadian Radarsat, and the newer German TerraSAR-X and Italian Cosmo-SkyMed. The traditional InSAR technique to detect surface deformation has been differential InSAR (DInSAR) – for example, see Eneva (2010) for an overview. However, DInSAR does not work in agricultural areas like Imperial Valley. A recent innovation, PSInSAR™ (e.g., Ferretti et al., 2007), and its extension, SqueeSAR™ (Ferretti et al., 2011), makes it possible to detect deformation also in such areas, although heavily vegetated areas (e.g., forests) still remain inaccessible to all techniques. Both PSInSAR and SqueeSAR make use of so-called "permanent scatterers" (PS), which are buildings, fences, lamp posts, transmission towers, rock outcrops, points aligned along roads and canals, etc. Such points serve as reflectors of the radar waves and are identified in a sequence of radar scenes, so that time series of surface deformation are derived at each individual PS. In addition, SqueeSAR makes use of "distributed scatterers" (DS). These are homogeneous areas emitting signals with smaller signal-to-noise ratios than the PS, but still significantly above the background noise. DS include rangelands, pastures, and bare earth, characteristic of relatively arid environments and rural areas. In this case the time series are assigned to the geometric centers of the DS areas.

Similar to using a reference (datum) point in leveling surveys, the PSInSAR/SqueeSAR measurements are relative to a reference point as well, so only local movements are detected. The deformation is first measured in the line-of-sight (LOS) to the satellite. Negative and positive LOS displacements indicate movements away from and toward the satellite, respectively. Deformation time series are obtained at each PS and DS and are used to calculate annual deformation rates from the slopes of straight lines fitted to the time series. Two sets of scenes are generally available, where the satellite moves north to south (descending) and south to north (ascending). This makes it possible to decompose the two sets of LOS movements into vertical and horizontal components. The satellite orbital geometries are such that only the east horizontal component can be obtained, while the north component remains nearly invisible to InSAR. The SAR instruments on board of the commonly used satellites are right-looking, in direction perpendicular to the satellite trajectory, and downward under a steep look (incident) angle from the vertical to the ground. This leads to LOS movements, which are significantly more sensitive to vertical displacements than to the east horizontal ones. Thus LOS movements away from or toward the satellite are often indicative of relative subsidence or relative uplift, respectively. For this reason, the LOS and vertical deformation maps often display similar spatial patterns, even if the numerical values are different. This was frequently observed at geothermal fields (e.g., Eneva et al., 2012, 2013b), where we have not observed horizontal movements larger than the vertical ones. However, if the horizontal movements significantly exceed the vertical ones (e.g., by more than three times for Envisat), the LOS deformation maps become more indicative of the horizontal displacements - this was demonstrated around strike-slip faults (Eneva et al., 2013a).

## 3. Data

### 3.1 Satellite Data

We have previously applied the above techniques to scenes from the Canadian Radarsat-1 satellite (Eneva et al., 2009; Eneva and Adams, 2010), and the European ERS-1/2 and Envisat satellites (Eneva et al., 2011 - 2013). In Imperial Valley this work made it possible to observe subsidence, uplift and horizontal movements in all four geothermal fields, as well as around prominent faults in the area. In particular, two distinct subsidence bowls have been observed within the CalEnergy units of the Salton Sea geothermal field. The SAR instruments on all these satellites were C-band, denoting a wavelength of 5.6 cm. Here we describe the results from a SqueeSAR application to data from the German TerraSAR-X (TSX) satellite, which belongs to a new generation of satellites providing significantly better spatial resolution, higher precision and more frequent coverage. The SAR instrument on board of TSX is X-band, with a wavelength of 3 cm. The revisit time for this satellite is shorter, 11 days, compared with 35 days for Envisat and ERS and 24 days for Radarsat-1. (However, scenes are not necessarily acquired during each passage).

Due to limitations of cost (depending on study area size), at this time the TSX data were analyzed only over a small area, of size 42 km$^2$, on the territory of the Salton Sea geothermal field (Figure 2), even though the footprints of the scenes used, from ascending track 15 and descending track 68, covered significantly larger areas. Table 1 shows the attributes of the TSX data and for comparison, also shows those for the Envisat data used previously (Eneva, 2012). The look ($\delta$) and heading ($\theta$) angles are used for determining the sensitivity of the LOS movements to the vertical and horizontal components. Its value is measured with numbers between –1 and +1; the closer to 0, the lower the sensitivity. This comparison shows that although the sensitivity of the TSX LOS to vertical movements is slightly reduced compared with Envisat

**Table 1.** Attributes of TerraSAR-X and Envisat.

| Attribute | TSX | | Envisat | |
|---|---|---|---|---|
| Band | X | | C | |
| Wavelength | 3 cm | | 5.6 cm | |
| Revisit time | 11 days | | 35 days | |
| | *Ascending* | *Descending* | *Ascending* | *Descending* |
| Number of scenes | 20 (track 15) | 17 (track 68) | 33 (track 306) | 45 (track 356) |
| Period Covered | 08/2012-10/2013 | 08/2012-09/2013 | 12/2003-08/2010 | 02/2003-09/2010 |
| Period Duration | 1 y 2 m | 1 y 1 m | 6 y 8 m | 7 y 7 m |
| Look angle δ | 26.9° | 29.4° | 20.3° | 22.1° |
| Heading angle θ | 11.5° | 9.8° | 12.9° | 11.3° |
| LOS sens. to vertical | +0.89 | +0.87 | +0.94 | +0.93 |
| LOS sens. to E horiz. | –0.44 | +0.48 | –0.34 | +0.37 |
| LOS sens. to N horiz. | –0.09 | –0.08 | –0.08 | –0.07 |

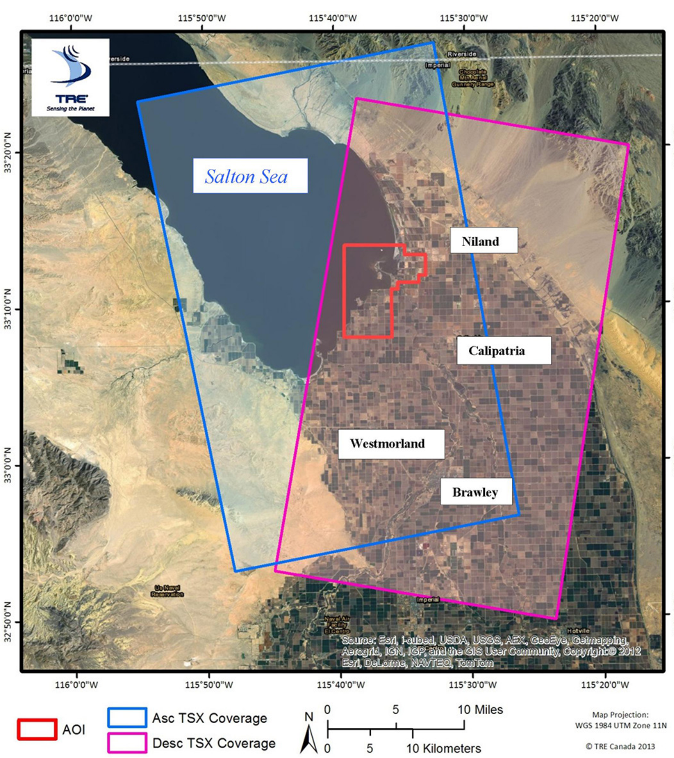


**Figure 2.** Footprints of the TerraSAR-X (TSX) scenes used in the analysis. The red outline marks the 42 km$^2$ study area.

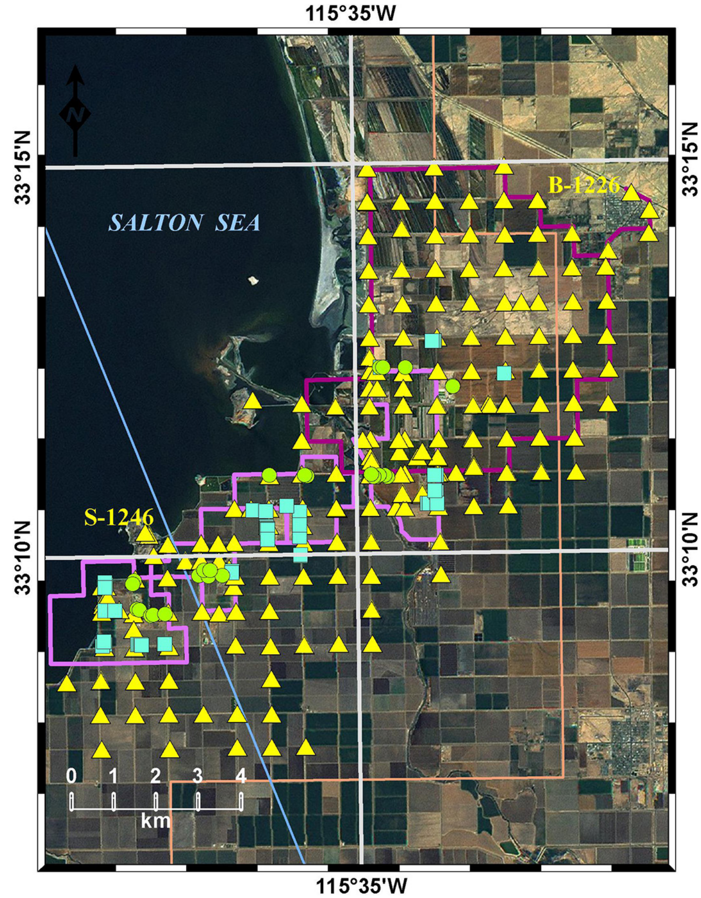


**Figure 3.** Locations of benchmarks and wells at the Salton Sea geothermal field. Yellow triangles – benchmarks. Green circles – production wells. Blue squares – injection wells. Pink polygons – CalEnergy units. Dark red – monitoring area with benchmarks by EnergySource. Light orange – Salton Sea KGRA (only a portion is seen). Blue line – central line through the Brawley Seismic Zone (BSZ).

LOS (by 4.9 % for the ascending and 5.9% for the descending orbits), there is a significant increase of sensitivity to the east horizontal movements (by 31 % for both the ascending and descending orbits). There is also a slight increase in sensitivity of TSX LOS to the north horizontal movements compared with Envisat LOS; however, both remain negligible.

### 3.2 Other Data

The surface deformation measured by SqueeSAR is compared with leveling data (i.e., vertical measurements). At the CalEnergy units of the field annual leveling data are available for the period 1998-2013. The number of benchmarks has increased over the years and as of 2013 has reached 108. The datum (reference) for these data is benchmark S-1246 on Obsidian Butte (southern Salton Sea shore). The 2012-2013 leveling data for the newly installed 94 benchmarks around the Hudson Ranch-1 development are referenced to benchmark B-1226. Figure 3 shows the locations of all leveling benchmarks at the two developments.

Furthermore, we use locations of production and injection wells and the monthly volumes of produced and injected fluid. These data were obtained from the Division of Oil, Gas and Geothermal Resources (http://www.conservation.ca.gov/dog/geothermal/). For the CalEnergy units there are data for 23 production and 36 injection wells. The percentage of total injected volume compared with the total produced volume is rather high. The data since February 1982 show that the average monthly percentage is 82%. During the period covered by the Envisat data, the average percentage was 77%, which increased to 84% for the TerraSAR-X period. The Hudson Ranch-1 wells are still confidential, so only locations but no fluid volumes are available for 5 production and 5 injection wells. The well locations for both developments are shown in Fig. 3, along with the leveling benchmarks.

**Table 2.** Numbers and density of PS and DS for TSX and Envisat.

| Attribute | TSX | | Envisat | |
|---|---|---|---|---|
| | *Ascending* | *Descending* | *Ascending* | *Descending* |
| **Number of PS** | 76,786 | 69,435 | 707 | 1,045 |
| **Number of DS** | 25,163 | 29,342 | 551 | 683 |
| **Total number of PS and DS** | 101,949 | 98,777 | 1,258 | 1,728 |
| **Density (points per sq. km)** | 2,427 | 2,352 | 30 | 41 |

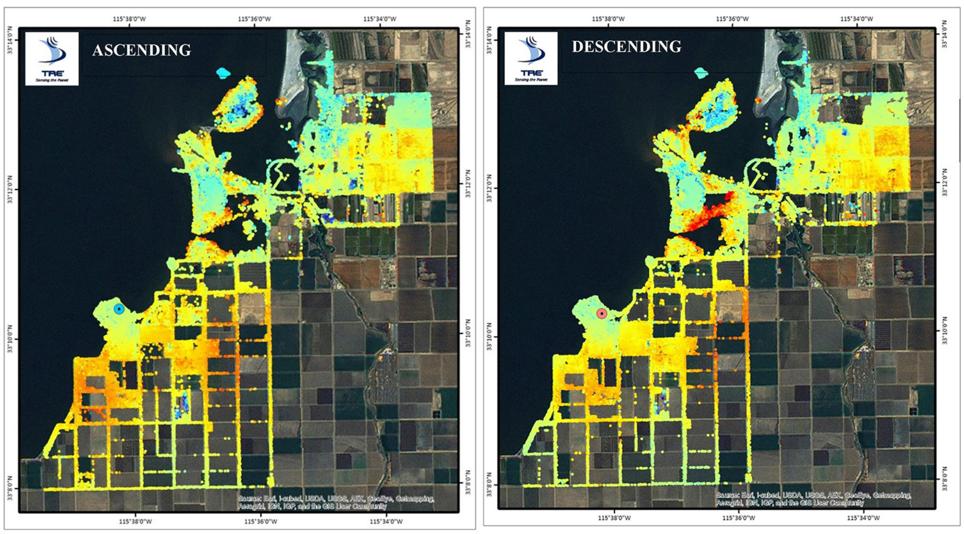


**Figure 4.** Deformation maps showing color-coded LOS annual rates from TSX. Color scale is from –40 mm/year (red) to +40 mm/year (blue), indicating movements away and toward the satellite, respectively (relative to S-1246).

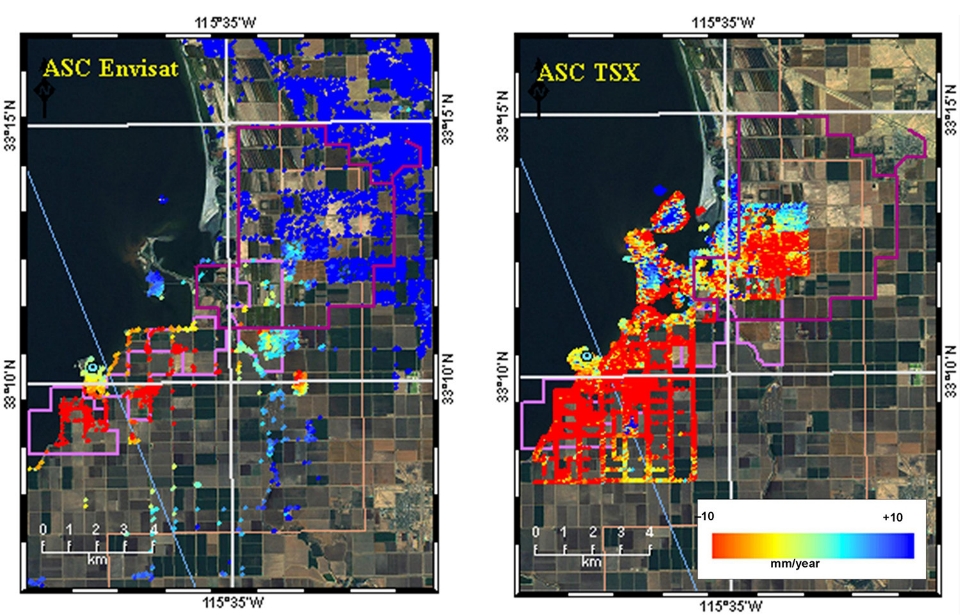


**Figure 5.** Ascending LOS Envisat and TSX deformation rates, color-coded according to the scale shown. CalEnergy and EnergySource areas marked as in Fig. 3. Blue circle with dot marks a location near the S-1246 benchmark, used as a reference in the SqueeSAR analyses.

## 4. Results

The TSX results presented here are referenced to the same leveling benchmark as before, S-1246, on Obsidian Butte. Although it is preferable for such points to be motionless, this is not possible to accomplish at the Salton Trough, especially on the southern shore of the Salton Sea. It was shown in our previous work (Eneva et al., 2009, 2012) that S-1246 experiences a significant subsidence of about –20 mm/year. This amount has to be added to the local movements if it is necessary to evaluate the absolute displacement in regional plan. Thus the maximum local subsidence of –30 mm/year observed at the CalEnrgy units of the Salton Sea geothermal field from the analysis of both the Radarsat-1 and Envisat data, translates to –50 mm/year of absolute movement. When the SqueeSAR results show uplift (relative to S-1246), often this still means subsidence, but slower than that of S-1246.

The TSX study area included at this time only a portion of the area that EnergySource started monitoring with leveling surveys around their new development. Their datum, benchmark B-1226, falls outside the TSX study area. It is not far from GPS station GRLS, for which "absolute" displacements are known. This, and other considerations from the earlier Envisat results covering most of the Imperial Valley (Eneva et al., 2012, 2013a), made it possible to establish that B-1226 is significantly more stable than S-1246, and is in a relative uplift of +18 mm/year compared with it (i.e., meaning only about –2 mm/year absolute subsidence). For the purposes of this TSX analysis, which used S-1246 as a reference, the leveling data from Hudson Ranch-1, originally using B-1226 as a datum, were re-referenced to S-1246.

Table 2 shows comparison of some statistics of the TSX and Envisat SqueeSAR results within the area used for the TSX analysis (the Envisat analysis was previously performed over a much larger area). The immediate important observation is the greatly increased density of PS and DS. The Envisat density is less than 2% of that for TSX in this particular area. Thus the SqueeSAR analysis produced ~80 times more ascending measurement points (PS and DS) and ~60 times more descending measurement points, even with a lower number of processed images within a shorter study period (see Tables 1 and 2).

Figure 4 shows the color-coded LOS rates (in mm/year) at individual PS and DS points from the ascending and descending TSX data. Both uplift and subsidence

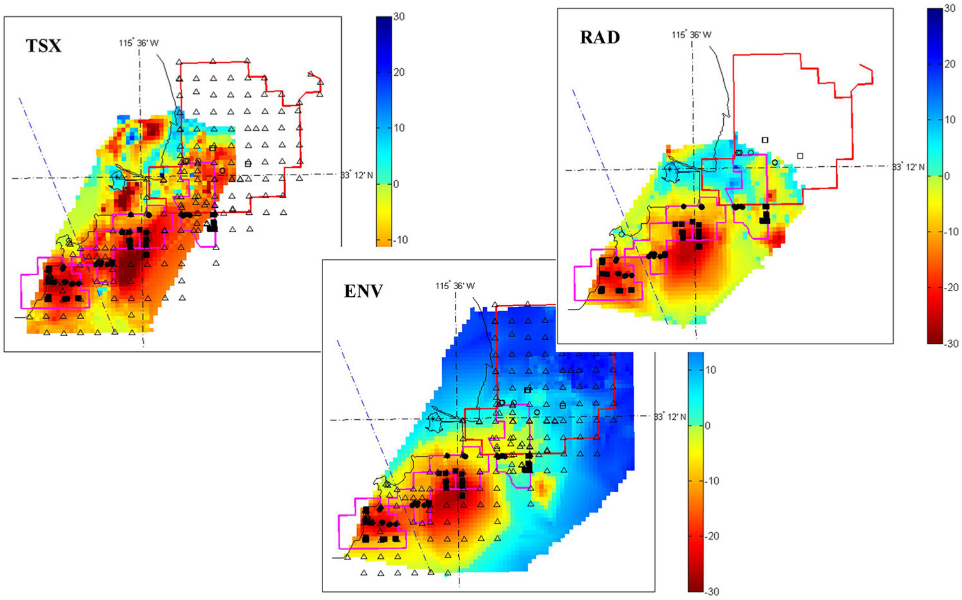


**Figure 6.** Comparison of interpolated decomposed vertical deformation rates from TSX, Envisat and Radarsat-1. Triangles – benchmarks, circles – production wells, squares – injection wells. Vertical rates are color-coded according to vertical bars on the right sides of the plots (mm/year). CalEnergy units (pink) and EnergySource (red) areas are outlined as in previous figures.

occurred, as observed previously in the Envisat results (Eneva et al., 2012, 2013a), with displacement rates ranging from −37 to −42 mm/year in the ascending LOS and −40 to −57 mm/year in the descending LOS. Most subsidence rates greater than −50 mm/year are concentrated near Red Island in the descending LOS. In some cases the deformation rates also reflect the local agricultural activity, as visible in the patchwork pattern in the northeastern portion of the area. The grid-like distribution elsewhere is due to the concentration of PS and DS along roads and canals, passing between agricultural fields, which were too variable during the study period to produce PS and DS.

The Envisat results previously showed that subsidence takes place beyond the limits of the producing CalEnergy units of the Salton Sea, such as in the vicinity of Hudson Ranch-1, although at a smaller rate than the observed maximum movements within the CalEnergy units (Eneva et al., 2013a) and the Obsidian Butte reference point (S-1246). Therefore, in the Envisat results these areas appeared in a relative uplift. Since the HR-1 operation only started in early 2012, the Envisat 2003-2010 results provide a pre-production baseline, while the TSX results for the period August 2012-October 2013 capture the time after the start of the production. In this case there exists the unique opportunity to compare the Envisat (2003-2010) rates with the TSX (2012-2013) rates for both the CalEnergy units and the new development of EnergySource. This may address the issue of whether surface changes are due to tectonic or anthropogenic reasons, or both. We have previously made an argument for primarily tectonic reasons, based on information available at that time (Eneva and Adams, 2010).

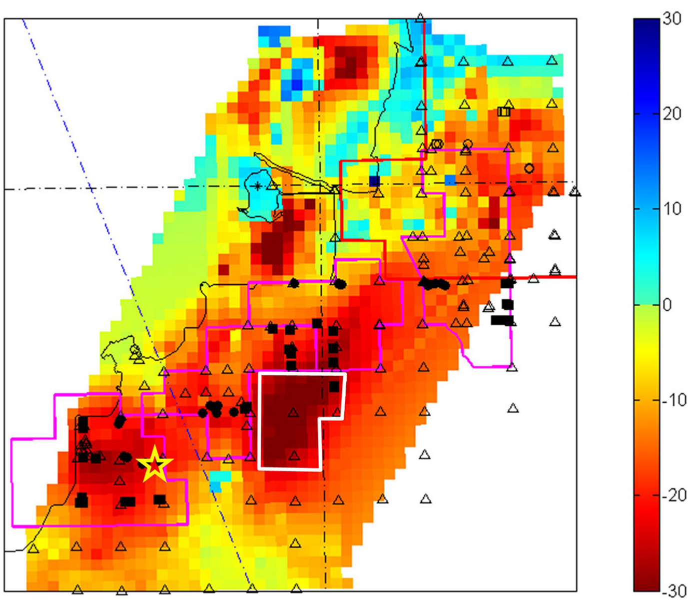

**Figure 7.** TSX vertical deformation map showing a polygon used to calculate average time series and rates next. Map is the same as in the leftmost panel in Fig. 6. Yellow star marks the location of a M5.1 epicenter in September 2005. Other notations like in previous figures.

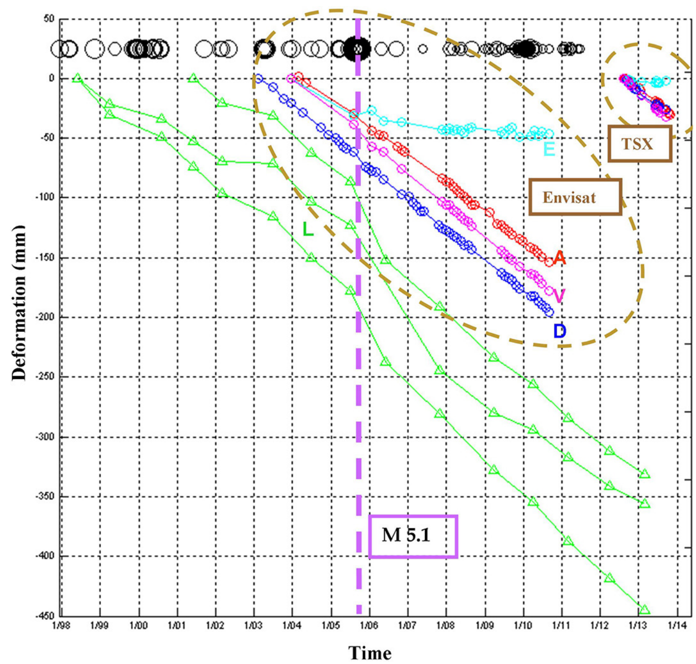


**Figure 8.** Mean time series from Envisat and TSX for the polygon in the CalEnergy units of the Salton Sea geothermal field from Fig. 7. Red (A) – mean ascending LOS time series, blue (D) – mean descending LOS time series, pink (V) – decomposed vertical, light blue (E) – decomposed east horizontal, green – leveling time series, purple – occurrence time of a M5.1 event in the fall of 2005. Black circles mark the occurrence times of earthquakes within the polygon. Brown ellipses outline time series from Envisat and TSX.

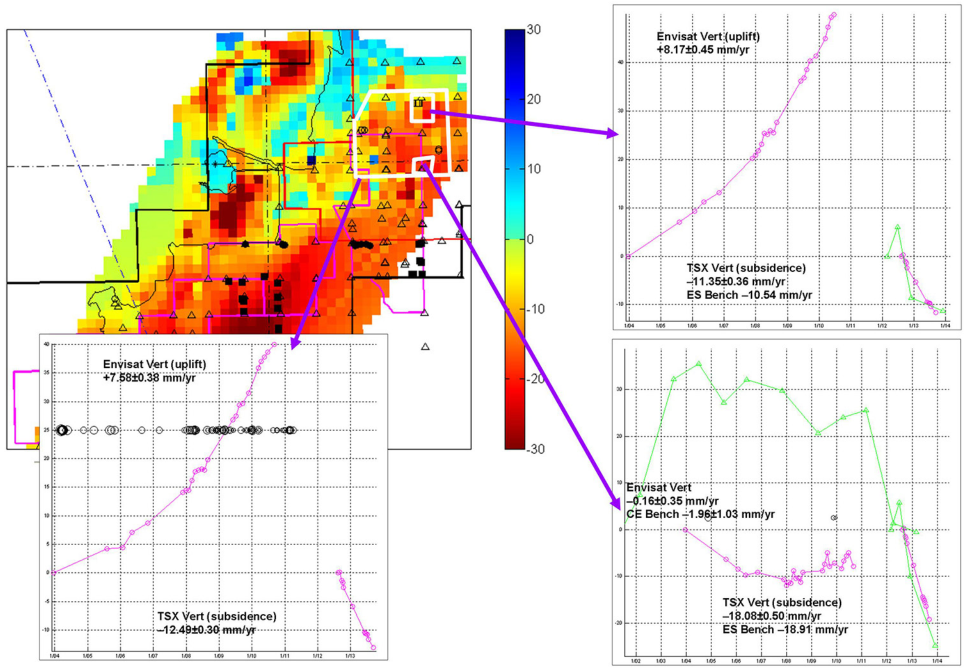


**Figure 9.** Comparison of TSX and Envisat vertical rates on the territory of the EnergySource development. TSX vertical deformation map is the same as in Figs. 6 and 7. White polygons mark areas, for which the vertical deformation time series from both satellites are shown. Leveling time series (green curves) are also shown for the two small polygons. They are omitted for the large polygon to avoid crowding of the plot from too many benchmarks. Wells are marked with empty symbols (circles for production and squares for injection) to indicate that they are still confidential – i.e., only their locations are known, but not the monthly volumes of production and injection. Empty triangles mark the locations of leveling benchmarks.

Figure 5 shows a comparison between the ascending LOS deformation maps from TSX and Envisat, which clearly show the significantly greater density of PS and DS from TSX, providing unprecedented detail never seen before. Figure 6 shows the interpolated decomposed vertical movements from TSX, Envisat and Radarsat-1. The Envisat and Radarsat-1 deformation maps appear smoother, but this is due to much larger areas of linear interpolation through areas without PS and DS compared with TSX. While the two subsidence bowls at the CalEnergy units appear in all three maps, one discrepancy stands out – to the northeast, the Envisat "blue" areas (uplift relative to S-1246, indicative of subsidence slower than that of S-1246) appear "red" in the TSX map. This qualitative observation becomes clearer next. Figure 7 shows the same map of the TSX vertical rates as in Fig. 6, with a polygon chosen to encompass the largest subsidence in the CalEnergy units. Mean time series are calculated for this polygon from both the Envisat data (2003-2010) and TSX data (2012-2013). These are shown in Figure 8, along with leveling time series from the benchmarks in this polygon. Comparing the time series of decomposed vertical movements from SqueeSAR (pink lines) with the leveling time series (green curves), the slopes of the curves are very similar, and hence, the rates are similar. Also, the Envisat and TSX vertical deformation time series appear parallel, hence the rates for the two periods are similar.

When the numerical values are compared, the TSX rate is in fact slightly higher, at ~–30 mm/year versus ~–28 mm/year from Envisat. Nonetheless, the main observation is that the most rapidly subsiding area within the CalEnergy units continues to subside at a comparable rate, when the periods December 2003 – October 2010 (from Envisat) and August 2012 – October2013 (from TSX) are compared. This holds true for all other areas in the CalEnergy units of the field. We note that when talking about the leveling rates during the Envisat period of 2003-2010, we mean the long-term rates, ignoring the downward slip observed at some benchmarks between the leveling before and after a M5.1 earthquake, which occurred on the territory of the CalEnergy units in September 2005. This change was not captured by the SqueeSAR LOS time series, due to inability to adjust unwrapping when there is lack of data.

Figure 9 focuses on areas around the new development by EnergySource. Two small and one larger areas are considered (white polygons). The figure shows only the vertical deformation time series (pink lines) to avoid crowding of the plots. The numerical values of the rates from these time series and the leveling benchmarks are also shown. The leveling measurements from the EnergySource benchmarks are re-referenced to S-1246. The observations here are very different from those for the CalEnergy units. The vertical time series from Envisat (i.e., pre-production) show uplift (relative to S-1246) in two of the areas and not much change in one of the smaller areas. However, significant subsidence takes place during the period covered by the TSX data, August 2012 – October 2013. There is good agreement between the SqueeSAR vertical rates and those measured in the leveling surveys (also marked on the plot). The maximum subsidence noted in this area is –18 mm/year. This is smaller than the maximum of –30 mm/year observed in the CalEnergy units, but represents a significant reversal of trend compared with the pre-production period. The monthly volumes of production and injection fluids are still confidential for the wells in this area. Nonetheless, the inevitable conclusion is that the surface deformation during the pre-production period (relative uplift) is very different from the subsidence observed after the operation of HR-1 started. The question raised by this observation is if this timing is coincidental, or it indicates anthropogenic reasons for subsidence.

## 5. Discussion

There are several arguments for non-anthropogenic reasons for surface deformation observed on the territory of the Salton Sea geothermal field. First, there are tectonic reasons for ongoing spreading and subsidence of the whole region, as previously discussed by Eneva and Adams (2010). More specifically, the deformation rate of –20 mm/year on Obsidian Butte may reflect the regional tectonic subsidence, while the additional subsidence of up to –30 mm/year observed at the CalEnergy units of the field may be due to deformation associated with pull-apart basins formed by a localized network of strike-slip and normal faults. This line of reasoning is supported by the fact that only a small portion of the total vast geothermal resource has been exploited so far. Also, the resource volume is unconfined, occurs at a significant depth (greater than a mile), and is highly fractured, but otherwise situated in a hard rock with very low porosity. Production and injection wells reach 7,000-9,000 ft under ground and the fractures extend for many thousands of feet below the bottom of the wells. For these reasons, geothermal operations at this particular field may not produce surface deformation, unlike geothermal production in much smaller, confined, consolidated, highly porous, and low-fractured reservoirs elsewhere. Tectonic reasons for subsidence are supported by observations of faults from seismic reflection studies in the Salton Sea (Brothers et al., 2009) to the north of the study area, and by a recent GPS-based geodetic study and strain modeling (Crowell et al., 2013). If there were evidence for insignificant changes of fluid levels and pressures in the wells, it would additionally boost the purely tectonic hypothesis for surface deformation. However, we do not have access to such data at this time, and therefore, while regional tectonic subsidence is known to be present, there is no proof that the additional amounts of subsidence at the geothermal field can be accommodated exclusively by local tectonics.

Another argument for non-anthropogenic effects is the observation that the subsidence at both the CalEnergy units and around the new development of Hudson Ranch – 1 (HR-1) by EnergySource is not associated with production wells in any obvious way, and is also observed away from the wells. This lack of association concerns both the well locations and the monthly fluid volumes. In fact, the largest subsidence at the CalEnergy units is around some of the injection wells. Thermal contraction due to cooling around the injection wells could be invoked in this case as an anthropogenic effect (Gary Oppliger, personal communication), but some modeling results indicate that it may be orders of magnitude smaller than the effect of changing pressures and fluid levels (Josh Taron, USGS, personal communication). In any case, changes in all three parameters are unknown at present.

Although lack of correlation between surface deformation and well locations and fluid volumes may be considered as indicative of non-anthropogenic reasons for surface deformation, it is notable that spatial separation between wells and surface effects has been observed in other areas, where there are no doubts about the anthropogenic origin of deformation. For example, at the Heber geothermal field, a subsiding area turned to uplift when injection was ramped up. However, this uplift occurred at a distance of about 2 km from the cluster of injection wells (Eneva et al., 2013b). In this case there was clear connection between the time series of leveling and monthly injection volumes, despite the substantial spatial separation. Although Heber is a different resource compared with the Salton Sea geothermal field, this example demonstrates the possible role of complicated fracture networks underground, which can lead to anthropogenic effects away from the wells.

Further doubts about the possibility of anthropogenic effects are related to the fact that the new HR-1 development has only one ~50 MW plant at this time, compared with the combined 327 MW from 10 CalEnergy plants, so it is difficult to associate the observed widespread effect on surface deformation with such relatively low production.

The above arguments for non-anthropogenic reasons for the deformation observations are challenged by the timing of the trend reversal, which is seen only on and around the territory of the new HR-1 development, while surface deformation in the CalEnergy units is similar in the periods 2003-2010 (from Envisat) and August 2012-October 2013 (from TSX). There are several non-anthropogenic effects to consider in this respect, for which dramatic change should have started between the two periods, i. e., after some time in 2010. These include: earthquake activity, which sometimes causes surface deformation; the receding Salton Sea and related exposure of fumaroles, which used to be submerged underwater (Lynch et al., 2013); and changes in agricultural activities, which can lead to soil compaction if irrigation is diminished. Below we discuss briefly our state of knowledge on these subjects.

First, there was indeed a swarm of seismic activity in this area in February 2012, which might have produced a surface deformation pattern different from that before the swarm. This can happen due to an abrupt co-seismic offset and/or aseismic creep for some period after the larger events in a swarm. In this case six events were with magnitudes M≥3, with the largest event of M3.4 occurring later in the sequence, on February 29. Such events are generally too small to cause surface deformation, especially a large and sustained change from the previous trend as the observed one. The latter would have to be attributed to a post-seismic creep still occurring long time after these earthquakes, as the TSX data started six months later (August 2012) and covered 14 months from that time on. We checked the GPS stations in the larger vicinity, such as GLRS, P507, CRRS, and DHLG, and none of them show any sudden offsets or continued aseismic movements. There was another, more substantial swarm to the south, near Brawley, with a maximum magnitude of M5.4, which started in late August 2012. However, it was too far to affect the surface deformation around HR-1. Its effect was observed at some GPS stations and at the local leveling benchmarks, but not as far to the north. Thus, in the absence of additional evidence to the contrary, earthquake activity appears an unlikely explanation of the timing of the observed trend reversal in the surface deformation around HR-1.

Furthermore, the receding Salton Sea is associated with drying up of the soil, and related subsidence. Figure 10 shows that the distribution of the TSX PS and DS points outlines the changing shore clearly. Two areas are shown separately: the northern part (top) including Mullet Island, the Alamo River delta, Red Island, and Rock Hill; and the southern part (bottom), including Obsidian Butte and an area along Lake Road. The background optical image is from 2012. Since the PS and DS points from TSX are with much higher density than those from Envisat, it is possible to observe a clear shoreline along the northern portion of the study area. The size of the Alamo River delta has increased significantly over time, especially in the area near Mullet Island (white polygon in top panels). The shoreline along Red Island (black dashed polygon, top) also experienced a large change, as has the area between Red Island and Rock Hill (white ellipse, top). In contrast, in the southern part of the area, most of the shoreline appears to remain the same (bottom), with the exception of Obsidian Butte (white ellipse) and a few small additional areas (white dashed circles). A drastic acceleration of the receding process after 2010 perhaps could explain the timing of the observed trend reversal. However, so far we have been unable to obtain information on the time series

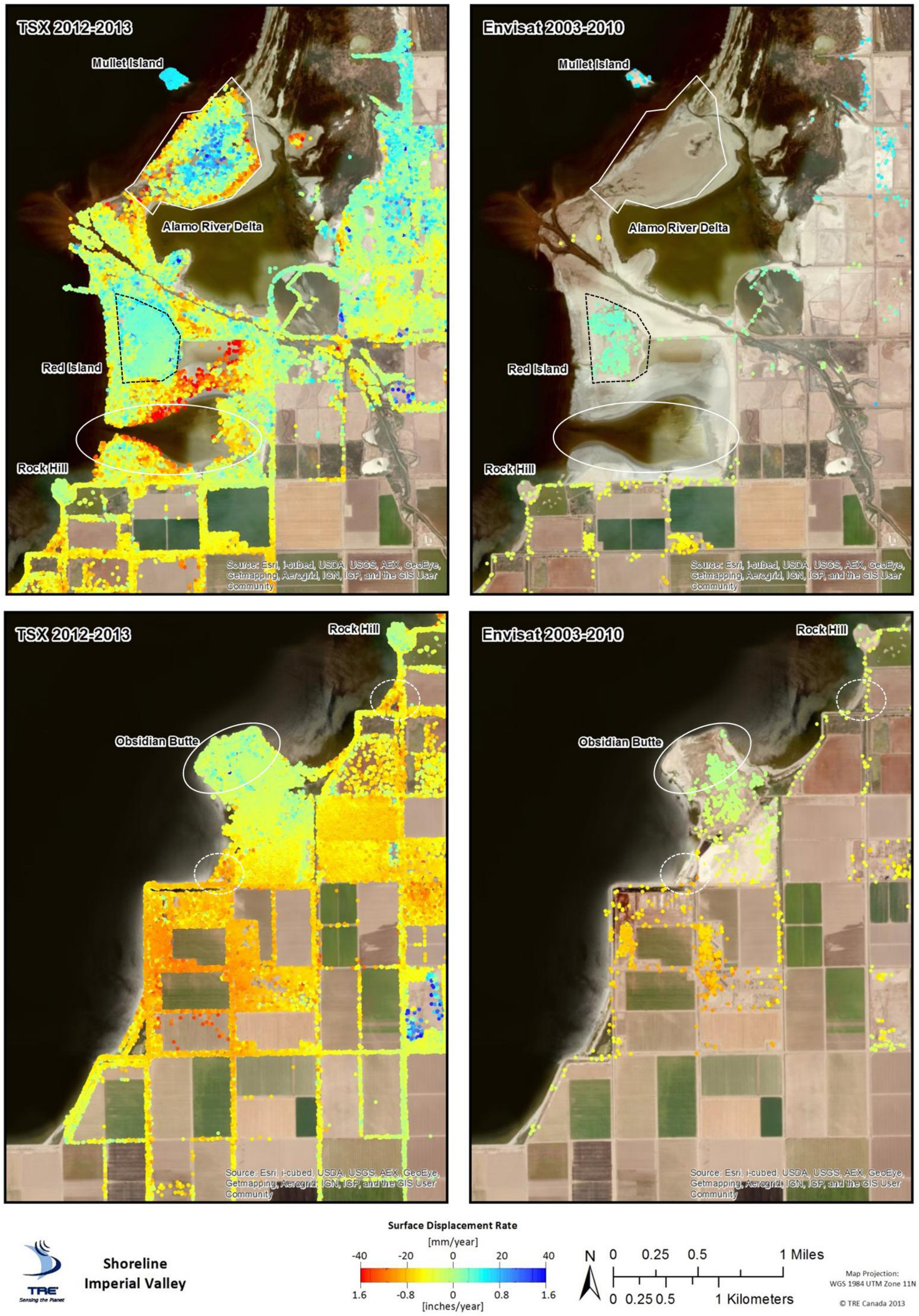


**Figure 10.** Comparison of TSX and Envisat along the southern shore line. Top – northern part. Bottom – southern part. Polygons and ellipses are explained in text.

of shoreline changes (we have inquired with the Imperial Irrigation District) and thus there is no evidence that the receding process has dramatically speeded up at that time, compared with previous years. Also, the observed trend reversal in the TSX results does not affect only the shore line, but inland areas as well. Thus this effect, although potentially important, is of unclear significance in the context of the observed trend reversal and its timing in particular.

Related to the receding of the lake shore are the newly exposed fumarole complexes (Lynch et al., 2013), which used to be submerged under water, but then started undergoing surface exposure around 2007. The fumarole fields occupy areas of 1000 to ~50,000 m$^2$, and consist of hundreds of mud volcanoes, mud pots, and gas vents. In particular, a rapid increase was observed in the number of sulfur vents over an eight-month period between January and September 2011. However, the SqueeSAR analysis identifies PS points only in areas, which appear the same from one satellite scene to another, even when undergoing displacement. That is, features with rapidly changing appearance are unlikely to be captured. In any case, this subject warrants revisiting in the future.

Finally, it would be informative to examine details of the agricultural patterns in the area around HR-1, such as changes in irrigation. At present, we do not have information on this subject, but it appears that widespread simultaneous decrease in irrigation (hence soil compaction and subsidence) after 2010 would be required to explain the timing of the trend reversal, and it would have to occur around HR-1, but not around the CalEnergy units.

In light of the above, the subject of tectonic versus anthropogenic contributions to the surface deformation at the Salton Sea geothermal field remains open. The reason is that although the timing of the observations can be interpreted to suggest a man-made effect, several possible non-anthropogenic factors need further investigation.

## 6. Conclusions

The InSAR technique used in this work, SqueeSAR, as applied to satellite data, is very effective in detecting surface deformation in agricultural areas, such as that of the Salton Sea geothermal field in southern California. The new generation of satellites, such as TerraSAR-X, assures much better spatial resolution, higher precision, and more frequent temporal coverage compared with older satellites. We presented surface deformation maps and mean deformation time series in polygons of interest, and compared them to observations from annual ground-based leveling surveys. It was possible to compare these for two periods, 2003-2010 (Envisat) and August 2012 – October 2013 (TerraSAR-X). These periods are post-production for the CalEnergy units of the field, but are pre- and post-production for the new Hudson Ranch-1 development. When the two periods are compared, the ongoing subsidence in the CalEnergy units is observed to be sustained, but there is a significant difference in the new development, where a reversal of trend is observed post-production. However, the question of man-made versus non-anthropogenic reasons for surface deformation at that field remains unresolved at this time.

## 7. Acknowledgments

The opinions stated in this paper are only those of the authors and are not necessarily supported by any other party. Support from the Geothermal Grants and Loans Program of the California Energy Commission (CEC), Grant GEO-10-001, is gratefully acknowledged. The TerraSAR-X satellite data were obtained from the German Space Agency (DLR) as part of an approved research data proposal. David Krommenhoek from the Imperial County Department of Public Works (ICDPW) provided digital data from leveling surveys. Data for the production and injection wells were obtained from the Division of Gas, Oil and Geothermal Resources (http://www.conservation.ca.gov/dog/geothermal/). The paper benefited from a review by Jim Lovekin.

## References

Brothers, D.S., N. W. Driscoll, G. M. Kent, A.J. Harding, J. M. Babcock, and R. L. Baskin (2009), "Tectonic Evolution of the Salton Sea Inferred from Seismic Reflection Data," Nature Geoscience, 2, 581-584, doi: 10.1038/NGEO590.

Crowell, B. W., Y. Bock, D. T. Sandwell, and Y. Fialko (2013), "Geodetic Investigation Into the Deformation of the Salton Trough," J. Geophys. Res. 118, 5030-5039, doi:10.1002/jgrb.50347.

Eneva, M., D. Adams, G. Falorni, and J. Morgan (2013a), "Applications of Radar Interferometry to Detect Surface Deformation in Geothermal Areas of Imperial Valley in Southern California," in Proc. 38th Workshop on Geothermal Reservoir Engineering, Stanford University, Stanford, California, February 11-13, 2013, SGP-TR-198.

Eneva, M., D. Adams, G. Falorni, and J. Morgan (2013b), "Application of Radar Interferometry to Detect Subsidence and Uplift at the Heber Geothermal Field, Southern California," Geothermal Resources Council Transactions 37, 491-499.

Eneva, M., D. Adams, G. Falorni, and J. Morgan (2012), "Surface Deformation in Imperial Valley, CA, from Satellite Radar Interferometry," Geothermal Resources Council Transactions, 36, 1339-1344.

Eneva, M., G. Falorni, W. Teplow, J. Morgan, G. Rhodes, and D. Adams, D. (2011), "Surface Deformation at the San Emidio Geothermal Field, Nevada, from Satellite Radar Interferometry," Geothermal Resources Council Transactions, 35, 1647-1653.

Eneva, M. (2010), "Detection of Surface Deformation at Mining and Geothermal Sites Using Satellite Radar Interferometry (InSAR)," in Proceedings of the 44th U.S. Rock Mechanics Symposium and 5th U.S.-Canada Rock Mechanics Symposium, Salt Lake City, June 27-30, 2010.

Eneva, M. and Adams, D. (2010), "Modeling of Surface Deformation from Satellite Radar Interferometry in the Salton Sea Geothermal Field, California," Geothermal Resources Council Transactions, 34, 527-534.

Eneva, M., G. Falorni, D. Adams, J. Allievi, and F. Novali, (2009), "Application of Satellite Interferometry to the Detection of Surface Deformation in the Salton Sea Geothermal Field, California," Geothermal Resources Council Transactions, 33, 315-319.

Ferretti, A., G. Savio, R., Barzaghi, A. Borghi, S. Musazzi, F. Novali, C. Prati, and F. Rocca (2007), "Submillimeter Accuracy of InSAR Time Series: Experimental Validation," IEEE Transactions on Geoscience and Remote Sensing, 45, 1142-1153.

Ferretti, A., A. Fumagalli, F. Novali, C. Prati, F. Rocca, and A. Rucci (2011), "A New Algorithm for Processing Interferometric Data-Stacks: SqueeSAR," IEEE Transactions on Geoscience and Remote Sensing, 49 (9), 3460-3470.

Geothermal Energy Association (2014), "2014 Annual U.S. and Global Geothermal Power Production Report," GEA, pp. 25.

Lynch, D. K., K. W. Hudnut, and P. M. Adams (2013), "Development and Growth of Recently Exposed Fumarole fFelds Near Mullet Island, Imperial County, California," Geomorphology, 195, 27-44.

Rymer, M. J., J. Boatwright, L. C. Seekins, J. D. Yule, and J. Liu (2002), "Triggered Surface Slips in the Salton Trough Associated with the 1999 Hector Mine, California, Earthquake," Bulletin of the Seismological Society of America, 92, 13001317, doi:10.1785/0120000935.

Wei, M., D. Sandwell, and Y. Fialko (2009), "A Silent Mw 4.7 Slip Event of October 2006 on the Superstition Hills Fault, Southern California," Journal of Geophysical Research, 114, B07402, doi:10.1029/2008JB006135.

Wei, M., D. Sandwell, Y. Fialko, and R. Bilham (2011), "Slip on Faults in the Imperial Valley Triggered by the 4 April 2010 Mw 7.2 El Mayor-Cucapah Earthquake Revealed by InSAR," Geophysical Research Letters, 38, L01308, doi:10.1029/2010GL045235.

Williams, C. F., M. J. Reed, R. H. Mariner, J. DeAngelo, and S. P. Galanis (2008), "Assessment of Moderate- and High-Temperature Geothermal Resources of the United States," U. S. Geological Survey. Report No.: Fact Sheet 2008-3082.